Discrete element modeling of acoustic emission in rock fracture

Shunying Ji,[a] and Shaocheng Di[b]
State Key Laboratory of Structural Analysis for Industrial Equipment Dalian University of Technology, Dalian 116023, China

(Received 6 December 2012; accepted 17 January 2013; published online 10 March 2013)

Abstract The acoustic emission (AE) features in rock fracture are simulated numerically with discrete element model (DEM). The specimen is constructed by using spherical particles bonded via the parallel bond model. As a result of the heterogeneity in rock specimen, the failure criterion of bonded particle is coupled by the shear and tensile strengths, which follow a normal probability distribution. The Kaiser effect is simulated in the fracture process, for a cubic rock specimen under uniaxial compression with a constant rate. The AE number is estimated with breakages of bonded particles using a pair of parameters, in the temporal and spatial scale, respectively. It is found that the AE numbers and the elastic energy release curves coincide. The range for the Kaiser effect from the AE number and the elastic energy release are the same. Furthermore, the frequency-magnitude relation of the AE number shows that the value of B determined with DEM is consistent with the experimental data. [doi:10.1063/2.1302109]

Keywords acoustic emission, discrete element model, failure criteria, elastic strain energy, parallel bonding

In the fracture of brittle materials, the interior micro-fracture can generate elastic waves known as acoustic emission (AE), which is a key parameter to identify the time, location and intensity of potential fracture. With AE signals, the in-situ stress and damage in rock,[1] the stability of rock slope[2] and the seismicity behavior prior to an earthquake can be estimated.[3,4] Monitoring techniques based on AE have been widely applied in geotechnical engineering.

With both physical experiment and numerical simulation, AE event can be recorded and counted as AE number in the fracture of brittle materials. In previous studies, some links between AE number and material damage have been established theoretically.[3,5] Physical experiments have been performed to determine the AE characteristics under tensile and compressive tests,[6,7] triaxial test,[8,9] and three point bending test.[10,11] AE is detected only during the first loading, up to a given compressing stress state. If the previously applied stress level is exceeded, the AE events will occur again. This phenomenon is called the Kaiser effect, which is a basic feature for in-situ stress determination in rocks. Recently, some numerical models have also been developed to simulate the AE number in the rock breakage process with finite element analysis,[12,13] boundary element method,[14,15] fiber bundle model,[16,17] and discrete element model (DEM).[18–22]

In this letter, DEM is applied to simulate the failure of rock specimen under uniaxial compression. For the contact interaction between particles, the linear viscoelastic model with the Mohr–Coulomb friction law is adopted, as shown in Fig. 1(a). Here $m_{\rm A}$ and $m_{\rm B}$ are the masses of particles A and B, $K_{\rm n}$ and $K_{\rm s}$ are the normal and tangential stiffnesses, $C_{\rm n}$ and $C_{\rm s}$ are the normal and tangential damping coefficients, μ is the friction coefficient. Spherical particles are bonded to construct the rock specimen. A parallel bonding model is introduced to transfer the force and moment between bonded particles, as shown in Fig. 1(b). A disk between the two bonded particles with thickness L and diameter R is used to describe the bonding function. Here, x_i is the location tensor of particle or disk, $\boldsymbol{F}$ and $\boldsymbol{M}$ are the contact force and moment between bonded particles; the superscripts "n" and "s" indicate the normal and shear directions, respectively. The maximum normal and tangential stresses in the disk can be written as

$$\sigma_{\max} = \frac{-F^{\rm n}}{A} + \frac{|M^{\rm s}|}{I}R, \tag{1}$$

$$\tau_{\max} = \frac{|F^{\rm s}|}{A} + \frac{|M^{\rm n}|}{J}R, \tag{2}$$

where A, R, J and I are the area, radius, polar inertia moment, and inertia moment of the bonding disk, respectively.

The constitutive relation is plotted in Fig. 2. The particle behaves elastic under low strain. The bonded particles are damaged when the tensile or shear stress reaches its strength σ_0. Considering the heterogeneity in rock materials on the micro scale, the bonding strength can be described as a random variable.[13,23,24] Here, we set the bonding strength as a normal distribution to describe the inhomogeneity of rock material, the mean and standard deviation of bonding strength are set at 100 MPa and 10 MPa, respectively.

The breakage criterion with the maximum strain is set as $\varepsilon_{\rm b} = \alpha\varepsilon_0$, and the residual strength is $\sigma_{\rm r} = \beta\sigma_0$ as shown in Fig. 2. Zhu and Tang[24] set $\varepsilon_0 = \varepsilon_{\rm r}$ in the FEM simulation of rock failure. In the present study, we

[a] Corresponding author. Email: jisy@dlut.edu.cn.
[b] Email: dishaocheng@mail.dlut.edu.cn.

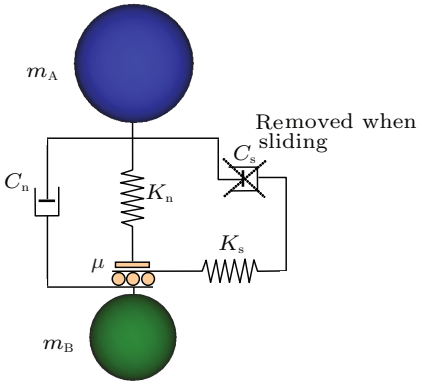

(a) Contact force model

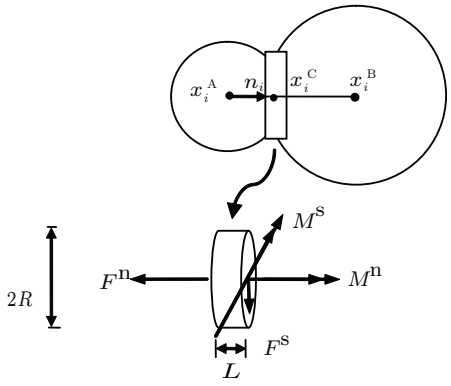

(b) Parallel bond model

Fig. 1. Contact and parallel bond force model for spherical elements.

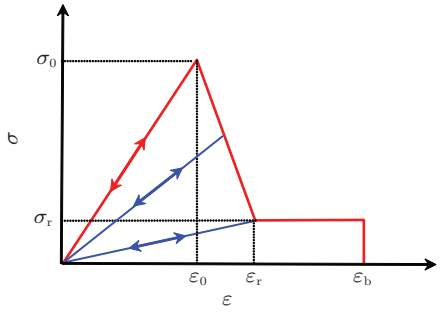

Fig. 2. Elastic damage constructive model of bonded particles in DEM simulation.

choose $\alpha = 2.0$, $\beta = 0.2$ and $\varepsilon_r = 1.2\varepsilon_0$. In the damaged materials, the elastic modulus can be defined as a linear function of damage factor D by $E = (1-D)E_0$. Here E and E_0 are elastic modulus of the damaged and the undamaged material, respectively. The damage factor D can be determined from the constitutive relationship as shown in Fig. 2.[13,24] The particle stiffness k_n is proportional to the elastic modulus as $k_n = \pi D_p E/4$, where D_p is the particle diameter.[25]

A cubic rock specimen is constructed with bonded spherical particles. The particles are randomly packed.

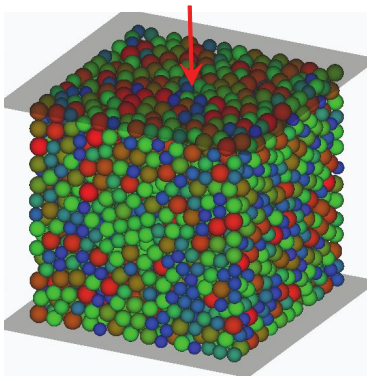

Fig. 3. Rock specimen described with DEM under uniaxial compression.

Any pair particles are bonded together when they contact in initial packing. The particle diameters are normally distributed in the range from $0.8\widetilde{D}_p$ to $1.2\widetilde{D}_p$, with the mean diameter $\widetilde{D}_p = 7$ mm. The elastic modulus is $E_0 = 30$ GPa, density is $\rho = 2\,500$ kg/m^3, particle friction coefficient is $\mu = 0.5$, and coefficient of restitution is $e = 0.5$. The time step is $dt = 7.5 \times 10^{-8}$ s in the simulation. The cubic rock specimen has a volume of 10 cm $\times$ 10 cm $\times$ 10 cm, constructed with 3 262 particles as shown in Fig. 3. The bottom load panel is fixed, and the top panel descents at a constant rate $u = 0.03$ m/s.

In this study, an acoustic emission event is triggered when a bond breaks. Two bonds within a critical separation L_c breaking within a critical duration T_c are considered to belong to the same acoustic emission event. The critical temporal period T_c depends on the fracture propagation time in the distance between two broken disks with a half shear wave velocity.[26] The critical length L_c is set as the distance of two contacted particles. Here, we plot the evolution of one AE event in the DEM simulation, as shown in Fig. 4. The relative particle number in this AE event is 2, 11, 30 and 86 at the time of 0.0, 9.6, 17.3 and 25.6 ms, respectively. Accordingly, the broken disk number is 1, 6, 19 and 61 at the relative time above.

The simulated stress–strain curve and the cumulative number of AE events are plotted in Fig. 5. The elastic modulus of the rock specimen is 9.67 GPa based on this curve in the linear elastic stage. From the cumulative AE number, it is obvious that the Kaiser effect lasts until strain $\varepsilon = 0.012$. The AE number represents essentially the degree of breakage in the rock specimen. The degree of breakage can be visualized by the structure of the force chains. The distributions of force chain are plotted in Fig. 6 at the strain $\varepsilon = 0.001$, 0.005, 0.010, 0.015, 0.025, respectively. The strength of force chain increases with the increase of strain and reaches its maximum when $\varepsilon = 0.015$, where the macro stress approaches its maximum. In this figure, both of the color and thickness of lines indicate the strength of force chains. The color of force chain represents the

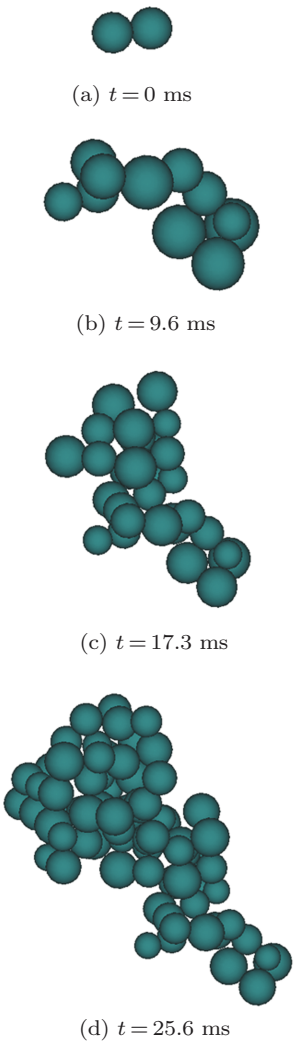

(a) $t = 0$ ms

(b) $t = 9.6$ ms

(c) $t = 17.3$ ms

(d) $t = 25.6$ ms

Fig. 4. Development of one AE event simulated with DEM.

strength with blue corresponding to small forces and red representing large forces. In the softening state after $\varepsilon = 0.015$, the force chains become weaken due to the breakage of the bonded particles. The breakage pattern of the specimen at $\varepsilon = 0.025$ is plotted in Fig. 6(f). The particles are colored in blue when their bonded disks are broken, and the intact particles are in red.

During compression, the potential elastic energy is restored in the deformation of elements in the rock specimen, which can be used to determine the released AE energy.[27,28] In the DEM simulation, the potential elastic energy can be written as[18,29]

$$E_{\mathrm{pe}} = \frac{1}{2}\sum_{i=1}^{N_{\mathrm{b}}}\left(\frac{|F^{\mathrm{n}}|^2}{K_{\mathrm{n}}} + \frac{|F^{\mathrm{s}}|^2}{K_{\mathrm{s}}} + \frac{A\,|M^{\mathrm{n}}|^2}{(JK_{\mathrm{s}})} + \frac{A\,|M^{\mathrm{s}}|^2}{(IK_{\mathrm{n}})}\right)_i, \tag{3}$$

where N_{b} is the number of broken bonds. The AE energy release can be determined as the difference of elastic potential energy before and after breakage of bonded

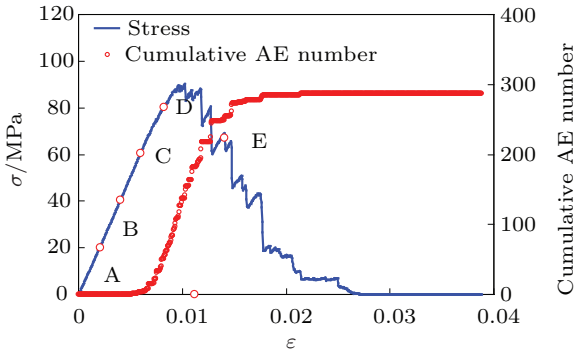

Fig. 5. Simulated cumulative AE number and normal stress with DEM of rock specimen.

particles. The released AE energy under the compression test is shown in Fig. 7. The trend of AE energy curve is close to that of the AE number. The similarity of the AE number and the AE energy is also found in the finite element method simulation.[27,28] Comparing the AE number and the AE energy release between Figs. 5 and 7, we see that they have the same Kaiser effect point at strain $\varepsilon_{\mathrm{K}} = 0.012$. Both of the AE number and AE energy approach zero when the stain is less than ε_{K}. After that point, both of the cumulative AE number and the AE energy increase with increasing strain. Therefore, the AE energy release is also a key factor to describe the AE characteristics.

In earthquake processes, the AE frequency-magnitude relation can be written as[8,18,30,31]

$$\lg N = a - bM, \tag{4}$$

where N is the number of earthquakes larger than magnitude. M, a and b are constants. This relation is also called Gutenberg–Richter relationship, which can be applied to study the acoustic emission characteristics in the laboratory tests. The magnitude of the AE is written as[8,18]

$$M = \frac{2}{3}(\lg \Delta E_{\mathrm{K\,max}} - 4.8), \tag{5}$$

where $\Delta E_{\mathrm{K\,max}}$ is the maximum value of AE energy in one AE event.

The parameter b is especially significant since it is used to analyze the pre-failure of rock materials. The parameter b usually varies between 1 and 2. It may depend on the rock type and its degree of heterogeneity, shear stress and confining pressure.[31] From triaxial compressive tests, the b value was found to lie in the range of 0.5–1.4.[9] In the previous DEM simulation of rock compression, the b value lied in the range from 0.9 to 3.3.[18,22] In this study, the AE frequency-magnitude relation is obtained based on the DEM simulation as shown in Fig. 8. The b value was determined as 2.29 for the portion of high AE energy.

From physical experiments, the AE signals as a kind of energy wave, are detected with sensors installed

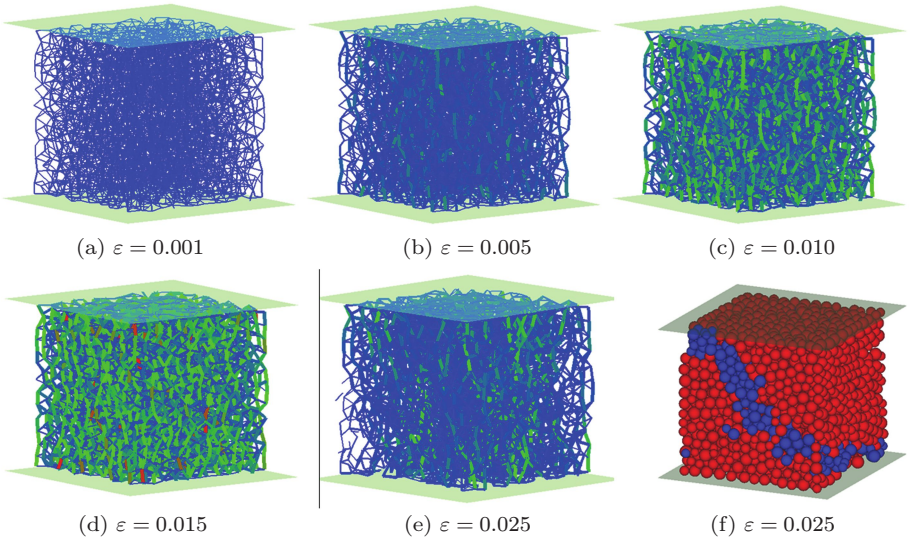

(a) $\varepsilon = 0.001$ (b) $\varepsilon = 0.005$ (c) $\varepsilon = 0.010$

(d) $\varepsilon = 0.015$ (e) $\varepsilon = 0.025$ (f) $\varepsilon = 0.025$

Fig. 6. Force chain distribution at different strains and the breakage of rock specimen at large strain.

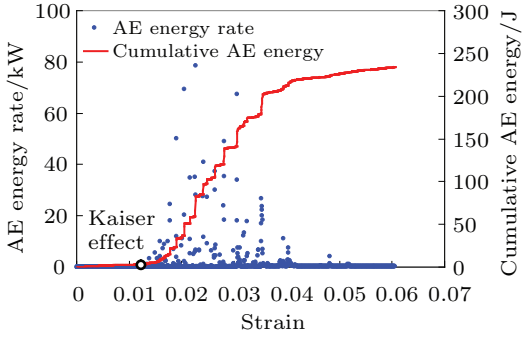

Fig. 7. The AE energy rate and cumulative AE energy simulated with DEM.

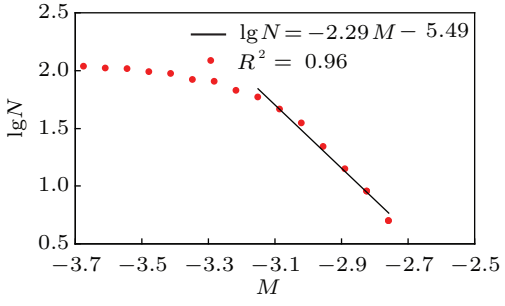

Fig. 8. Relation of AE frequency-magnitude simulated with DEM.

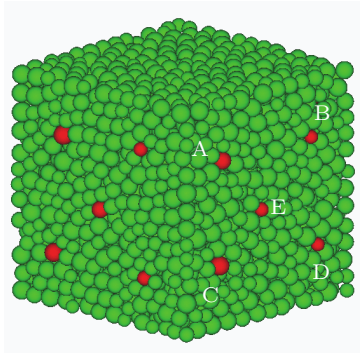

(a) Surface particles selected on the cubic specimen

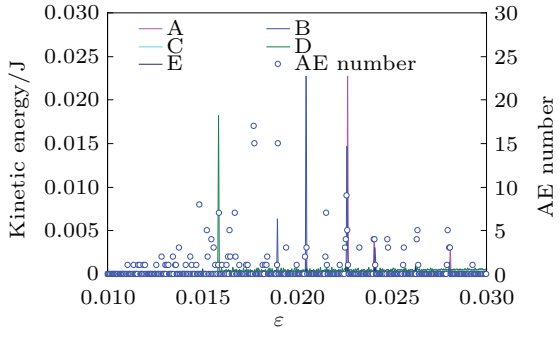

(b) Kinetic energy of surface particles and AE number

Fig. 9. Surface particles of the roe simple and its kinetic energy.

on the specimen surface.[6,7,9,10] To numerically emulate this, the kinetic energy of several surface particles is extracted from the DEM simulation to analyze their relation with the AE number. For the cubic rock specimen shown in Fig. 9(a), the kinetic energy of 20 surface particles is obtained. The kinetic energy of five particles shown in Fig. 9(a) is monitored and the results are plotted in Fig. 9(b). Each kinetic pulse in Fig. 9(b) corresponds to one AE event. Therefore, the kinetic energy of surface particles can present the occurrence time of AE event. But we can also find that some AE events may not have reached the five selected particles yet. If we select more surface particles, most of the AE events can be captured. The relationship between surface par-

ticle kinetic energy and AE number of rock specimen will be discussed in details with more simulated data in the following study.

In this study, some AE characteristics of rock fracturing, such as the Kaiser effect, AE energy release, and AE frequency-magnitude relation, are analyzed with DEM. To simulate precisely the AE characteristics of rock fracture with rational bonding strength and particle size, the comparison between DEM results and physical experiments will be performed to calibrate the numerical model in a future study. DEM simulations of acoustic emission in rock fracture can improve our understanding of the AE signals prior to geo-hazards, this improved understanding can lead to better application of AE technique for geo-hazard forecasting.

This work was supported by the National Basic Research Program of China (2010CB731502).

1. L. Qiao, Z. Zu, and K. Zhao, et al., Procedia Eng. **26**, 1473 (2011).
2. T. Shiotani, NDT & E Int. **39**, 217 (2006).
3. C. A. Tang, Z. H. Chen, and X. H. Xu, et al., Pure Appl. Geophys. **150**, 203 (1997).
4. A. Carpinteri, J. Xu, and G. Lacidogna, et al., Cement Concrete Comp. **34**, 529 (2012).
5. D. J. Holcomb, Int. J. Rock Mech. Min. **30**, 929 (1993).
6. S. T. Dai, and J. F. Labuz, J. Mater. Civil Eng. **9**, 200 (1996).
7. V. Rudajev, J. Vilhelm, and T. Lokajicek, Int. J. Rock Mech. Min. **37**, 699 (2000).
8. D. A. Lockner, J. D. Byerlee, and V. Kuksenko, et al., Nature **350**, 39 (1991).
9. X. Lei, K. Masuda, and O. Nishizawa, et al., J. Struct. Geol. **26**, 247 (2004).
10. C. S. Kao, F. C. S. Carvalho, and J. F. Labuz, Int. J. Rock Mech. Min. **48**, 666 (2011).
11. D. G. Aggelis, A. C. Mpalaskas, and D. Ntalakas, et al., Constu. Build. Mater. **35**, 183 (2012).
12. M. Aberg. Int. J. Solids Struct. **38**, 6643 (2001).
13. C. A. Tang, H. Liu, and P. K. K. Lee, et al., Int. J. Rock Mech. Min. **37**, 555 (2000).
14. M. Ohtsu, Y. Kaminaga, and M. C. Munwam, Constu. Build. Mater. **13**, 57 (1999).
15. A. Lavrov, A. Vervoort, and M. Wevers, et al., Int. J. Rock Mech. Min. **39**, 287 (2002).
16. R. CHidalgo, F. Kun, and H. J. Hermann, Phys. Rev. E **64**, 066122 (2001).
17. F. Bosia, N. Pugno, and G. Lacidogna, et al., Int. J. Solids Struct. **45**, 5856 (2008).
18. J. F. Hazzard, and R. P. Young, Int. J. Rock Mech. Min. **37**, 867 (2000).
19. A. Fakhimi, F. Carvalho, and T. Ishida, et al., Int. J. Rock Mech. Min. **39**, 507 (2002).
20. M. Cai, P. K. Kaiser, and H. Morioka, et al., Int. J. Rock Mech. Min. **44**, 550 (2007).
21. H. Su, C. H. Dang, and Y. J. Li, Rock Soil. Mech. **32**, 1886 (2011). (in Chinese)
22. S. Invernizzi, A. Carpinteri, and G. Lacidogna, et al., in: *Proceedings of the SEM Annual Conference*, Indianapolis, Indiana, 2010
23. S. Qin, S. Wang, and H. Long, et al., Int. J. Rock Mech. Min. **36**, 1073 (1999).
24. W. C. Zhu, and C. A. Tang, Constu. Build. Mater. **16**, 453 (2002).
25. S. Ji, and H. H. Shen, J. Rheol. **52**, 87 (2008).
26. J. F. Hazzard, and R. P. Young, Tectonophysics **356**, 181 (2002).
27. W. C. Zhu, X. D. Zhao, and Y. M. Kang, et al., Mater. Struct. **43**, 633 (2010).
28. S. Y. Wang, S. W. Sloan, and M. L. Huang, et al., Rock Mech. Rock Eng. **44**, 179 (2011).
29. Itasca. *PFC3D-particle Flow Code* (Itasca Consulting Group Inc., Minnesta, 2003).
30. A. Johansen, and D. Sornette, Eur. Phys. J. B **18**, 163 (2000).
31. G. Michlmayr, D. Cohen, and D. Or, Earth-Sci. Rev. **112**, 97 (2012).